The Canadian Mineralogist
Vol. 49, pp. 29-40 (2011)
DOI: 10.3749/canmin.49.1.29

DISSYMMETRIZATION IN TOURMALINE: THE ATOMIC ARRANGEMENT OF SECTORALLY ZONED TRICLINIC Ni-BEARING DRAVITE

JOHN M. HUGHES[§]

Department of Geology, The University of Vermont, Burlington, Vermont 05405, U.S.A.

JOHN RAKOVAN

Department of Geology, Miami University, Oxford, Ohio 45056, U.S.A.

ANDREAS ERTL

Institut für Mineralogie und Kristallographie, Geozentrum, Universität Wien, Althanstrasse 14, A–1090 Vienna, Austria

GEORGE R. ROSSMAN

Division of Geological and Planetary Sciences, California Institute of Technology, Pasadena, California 91125-2500, U.S.A.

IVAN BAKSHEEV

Geology Department, Lomonosov Moscow State University, Vorobiovy Gory, Moscow 119992, Russia

HEINZ-JÜRGEN BERNHARDT

Institut für Geologie, Mineralogie und Geophysik, Ruhr-Universität Bochum, D–44801 Bochum, Germany

ABSTRACT

Although putatively possessing hexagonal $R3m$ symmetry, reports of optically anomalous tourmaline are common, and recently an occurrence of triclinic tourmaline was reported with dissymmetrization that resulted from non-equivalency of the occupants of the Y sites. We report the atomic arrangement of Ni-bearing dravite from the Berezovskoe gold deposit, Middle Urals, Russia, in the non-conventional triclinic space-group $R1$ ($R = 4.41\%$) to facilitate comparison with the conventional tourmaline $R3m$ cell. The dissymmetrization occurs as a result of inequalities among both the hexagonally equivalent Y and hexagonally equivalent Z tourmaline sites. The atomic arrangement of this triclinic dravite demonstrates that the atomic arrangement of tourmaline is robust, and is capable of incorporating various substituents by modifying the putative hexagonal structure in lower symmetries, suggesting that further exploration of tourmaline's role in trace-element variation is warranted. Optical studies demonstrate the heterogeneous biaxial character of the crystals. Domains of different optical orientation and $2V$ correspond directly to trigonal prism $\{100\}$, $\{010\}$ and pedion $\{001\}$ sectors, indicating optical sectoral zoning. Compositional sectoral and concentric zoning are also observed within the crystals. Spectroscopic studies show the optical absorption spectrum of the Berezovskoe tourmaline has strong absorptions in the 400, 600–700, and 1100 nm regions, in addition to OH features near 1450, 2300, and 2700 nm. We conclude that the color in the $\mathbf{E} \perp \mathbf{c}$ polarization comes dominantly from Fe mixed-oxidation-state couples on the Y sites, and from Cr^{3+}. Contributions to the color from the nickel are believed to be minor and will fall in the regions of strong Cr and Fe absorption. The ordered arrangement of cations on the Y and Z sites and the correlation of optical orientation with specific sectors indicate that dissymmetrization occurs during growth by differential incorporation at structurally different atomic sites at the surface of the crystal, which in the bulk are symmetrically equivalent.

Keywords: tourmaline, optical sectoral zoning, dissymmetrization, triclinic, optical anomaly, dravite, Berezovskoe gold deposit, Russia.

[§] *E-mail address*: jmhughes@uvm.edu

SOMMAIRE

Quoiqu'ayant une symétrie putative hexagonale *R*3*m*, les indices de tourmaline optiquement anomale sont relativement communs, et un exemple de tourmaline triclinique a récemment été signalé dans lequel la dissymétrisation résulte de la non-équivalence des occupants des sites *Y*. Nous décrivons ici l'agencement des atomes dans la dravite nickelifère provenant du gisement aurifère de Berezovskoe, dans les Ourales moyennes, en Russie, en termes du groupe spatial non conventionnel triclinique *R*1 (*R* = 4.41%) afin de faciliter une comparaison avec la maille conventionnelle *R*3*m*. La dissymétrisation résulte des inégalités parmi les sites *Y* et *Z*, qui sont chacuns équivalents dans une maille hexagonale. L'agencement des atomes dans la dravite triclinique démontre sa robustesse, et sa capacité à incorporer divers substituants par modification de la structure hexagonale idéale par diminution de la symétrie, ce qui invite une évaluation élargie du rôle de la tourmaline pour expliquer les variations en éléments traces. Nos études optiques démontrent le caractère biaxe et hétérogène des cristaux. Les domaines différant en orientation optique et en 2*V* correspondent directement aux secteurs du prisme trigonal |100|, |010| et au pédion |001|, indiquant une zonation en secteurs. Une zonation sectorale et une zonation concentrique sont aussi observées dans ces cristaux. D'après nos études, le spectre d'absorption optique de la tourmaline de Berezovskoe montre de fortes absorptions autour de 400, 600–700, et 1100 nm, ainsi que des absorptions dues aux groupes hydroxyle près de 1450, 2300, et 2700 nm. Nous croyons que la couleur dans la polarisation $\mathbf{E} \perp \mathbf{c}$ provient surtout du Fe en couples mixtes de Fe^{2+} et Fe^{3+} aux sites *Y*, et du Cr^{3+}. Toute contribution du nickel à la couleur serait secondaire, et correspond aux régions d'absorption intense de Cr et Fe. La distribution ordonnée des cations aux sites *Y* et *Z* et la corrélation de l'orientation optique dans des secteurs spécifiques indiquent que la dissymétrisation serait causée par l'incorporation différentielle d'atomes aux sites structuralement distincts mais idéalement équivalents à la surface du cristal en croissance.

Mots-clés: tourmaline, zonation optique en secteurs, dissymétrisation, triclinique, anomalie optique, dravite, gisement d'or de Berezovskoe, Russie.

INTRODUCTION

Tourmaline is a common accessory mineral in igneous and metamorphic rocks, and is the most common accessory phase that sequesters boron in the Earth's crust. During the past decade, numerous studies of the crystal chemistry of tourmaline have been undertaken to elucidate this complex phase, one of the last common silicate minerals to undergo extensive crystal-chemical scrutiny. Tourmaline crystals are commonly compositionally zoned, exhibiting both concentric and sectoral zoning (Dietrich 1985, Henry *et al.* 1999, Akizuki *et al.* 2001, Rustemeyer 2003, van Hinsberg *et al.* 2006, van Hinsberg & Marschall 2007). Despite its putative *R*3*m* symmetry, numerous previous studies have noted biaxiality in tourmalines, as summarized in Shtukenberg *et al.* (2007). Several recent studies have demonstrated dissymmetrization in tourmalines in which different growth sectors show differences in optical orientation and other optical properties, referred to here as optical sectoral zoning (Akizuki *et al.* 2001, Shtukenberg *et al.* 2007). Akizuki *et al.* (2001) described sectorally distributed domains of trigonal, orthorhombic and triclinic optical character in tourmaline from a pegmatite in Jochy, Madagascar. They reported lattice parameters obtained by X-ray-diffraction methods from optically homogeneous fragments removed from these sectors. Variations in lattice parameters are attributed to compositional differences that are also observed among the sectors, *i.e.*, compositional sectoral zoning. Shtukenberg *et al.* (2007) reported an example of triclinic, optically sectorally zoned elbaite, and undertook structure studies of crystal fragments taken from a single |021| sector. They demonstrated that the dissymmetrization occurred solely from ordering of Al and Li occupants at the hexagonally equivalent *Y* sites.

In a recent study, Baksheev & Kudryavtseva (2004) reported on nickeloan dravite from the Berezovskoe gold deposit, Middle Urals, Russia. Here, we report the atomic arrangement, chemical composition, and optical and spectroscopic properties of that triclinic, compositionally and optically sectorally zoned crystal of dravite.

GEOLOGICAL SETTING

The mesothermal Berezovskoe gold deposit is located 10 km north of Ekaterinburg (Baksheev & Kudryavtseva 2004, Fig. 1). It occurs within the moderately eroded Berezovskii tectonic block, which is dominated by Lower Silurian volcanic and sedimentary rocks. The stratigraphic succession and the ultramafic bodies that it contains are cut by Lower Devonian gabbros; the succession is gently folded, dipping 20 to 30° to the west and northeast. The stratigraphic unit, ultramafic rocks and gabbros are weakly metamorphosed to greenschist-facies conditions.

At least three hydrothermal metasomatic associations (altered wallrock) and related quartz veins are recognized within the Berezovskoe gold deposit. The associations are believed to be successive and related to dikes. These are barren propylite, tungsten-bearing "gumbeite" and gold-bearing "beresite–listwanite". The alteration assemblages were developed in all pre-existing rocks, including metamorphic rocks, quartz monzonite, and dikes. Propylitic alteration formed at the expense of silicic to mafic rocks includes chlorite, epidote, tourmaline, amphibole, albite, quartz, carbonate minerals, and hematite. Propylitically altered ultramafic rocks contain talc, magnesite, and hematite. Veins within the altered rock contain quartz, magnesite, talc (including Ni-bearing talc), tourmaline (including Ni-bearing dravite) and green Cr-bearing muscovite. These altered rocks and veins are essentially free of gold.

Nickel-bearing tourmaline associated with Ni-bearing talc (up to 10.71 wt% NiO) and green Cr-bearing muscovite occurs within magnesite–quartz veinlets and veins in Uspenskaya Gorka, located in the eastern flank of the Berezovskoe gold deposit. The unusual compositions of the silicates reflects a Ni- and Cr-rich geochemical environment of mineralization, because the veins (5 cm to 3 m thick) are hosted in hematite – talc – carbonate alteration formed at the expense of ultramafic rocks. Tourmaline constitutes about 5% of the vein's volume. It is intergrown with quartz, indicating their simultaneous crystallization, and develops as isolated light and dark green needles up to one cm long or as aggregates of tourmaline needles.

According to the chemical data (Baskheev & Kudryavtseva 2004), the Ni-bearing tourmaline species are magnesiofoitite and dravite, the maximum Ni content being 3.96 wt% NiO. Tourmaline with a similar Ni content (up to 3.53 wt% NiO) was recorded by Henry & Dutrow (2001) from a metabauxite from Samos, Greece. The Ni content is distributed in an oscillatory and irregular fashion within the single crystals.

EXPERIMENTAL

Optical studies

A (001) section was cut from a prismatic crystal of dravite 3 mm long and 0.5 mm wide (Fig. 1); the crystal used in the optical studies was not the crystal used for single-crystal structure studies. The crystal exhibits two trigonal prisms {100} and {010} and broken terminations (the nomenclature of forms is based on the hexagonal cell). Other similar crystals exhibit terminations composed of {101} and {001} faces. The section (Figs. 2, 3) exhibits a sector distribution similar to that shown schematically in Figure 1B. Optical observations were made on a petrographic microscope in plane-polarized light (Fig. 3) and under crossed polars (Fig. 2). Estimates of the optic angle, 2*V*, were made using Mallard's method and the maximum separation of melatopes in *Bxa* interference figures. Oriented sections of quartz with known off-axis interference figures were used to calibrate angular values of separation. Optic signs were evaluated with an accessory gypsum plate and *Bxa* interference figures. Evaluation of the spatial relationships among growth sectors, concentric zones, and the external morphology were made using the program SHAPE (Ver. 7.2).

Optical absorption spectra were obtained by combining spectra obtained with a diode-array spec-

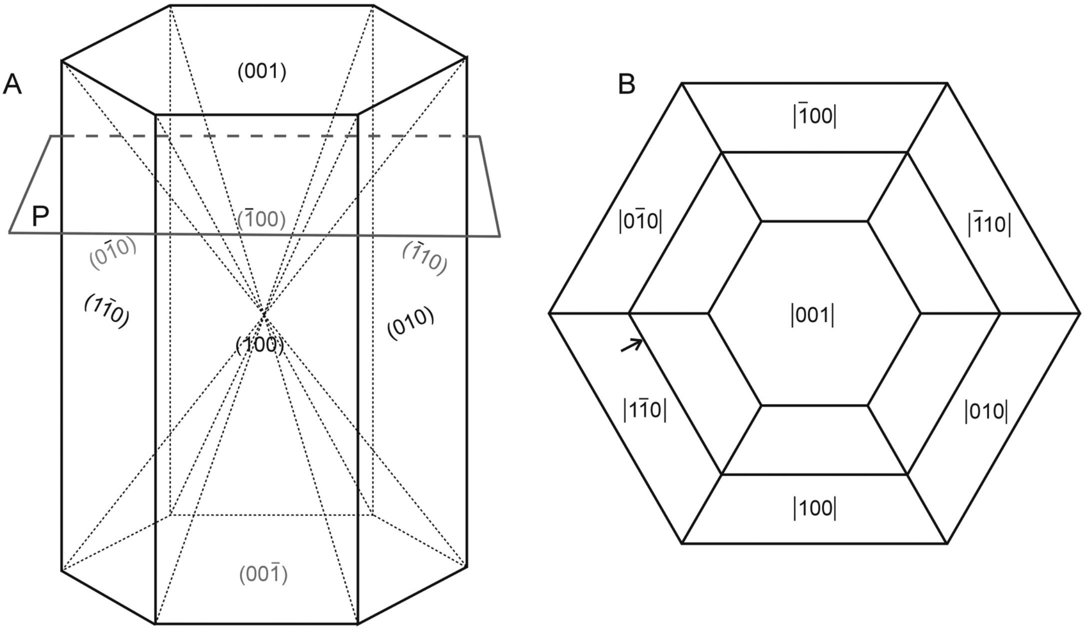

FIG. 1. A) Schematic drawing of the tourmaline crystal used for optical measurements showing trigonal prism {100}, {010} and pedion {001}, $\{00\bar{1}\}$ faces and sectors. The plane P indicates the rough position of a (001) section taken from the crystal. B) Schematic drawing of the (001) section indicating the sectors |*hkl*| present. The hexagon indicated by the arrow represents a dark concentric zone seen in Figures 2 and 3. Note that the nomenclature of forms refers to hexagonal cell.

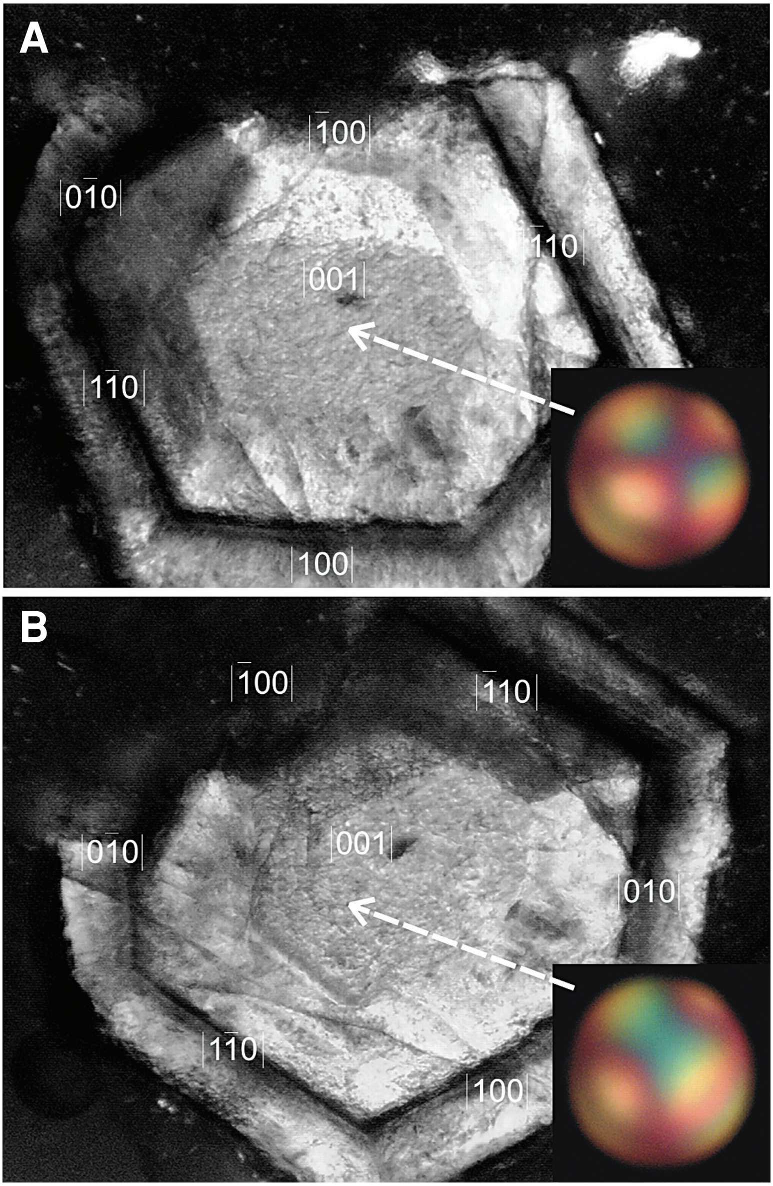

FIG. 2. A (001) section of Ni-rich dravite under crossed polars. A) Orientation 1, in which the |0$\bar{1}$0| and |1$\bar{1}$0| sectors are close to extinction, whereas other sectors are not. Inset in lower right corner is an interference figure taken within the |001| sector with a gypsum plate inserted. B) Orientation 2, in which the |$\bar{1}$00| and |$\bar{1}$10| are close to extinction, whereas other sectors are not. Inset in lower right corner is a biaxial negative interference-figure taken within the |001| sector with a gypsum plate inserted. The 2*V* is approximately 4°.

trometer described in Ertl *et al.* (2008) in the 390 to 1600 nm region, with spectra obtained on a Thermo-Nicolet Magna 860 FTIR with a Continuμm$^{\mathrm{TM}}$ infrared microscope with a MCT–A detector (1200 to 3000 nm) and LiIO$_3$ crystal polarizer.

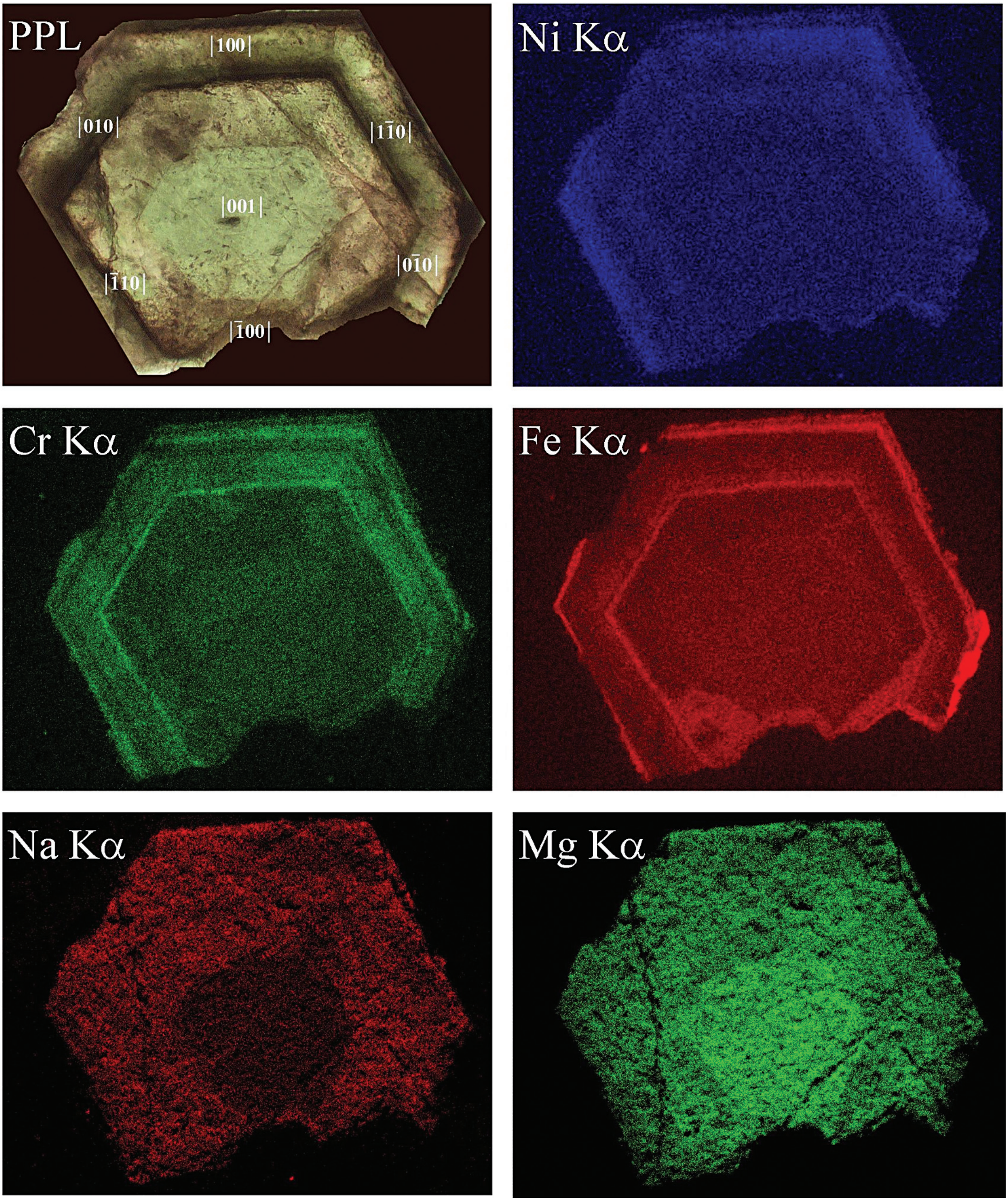

FIG. 3. The (001) section of Ni-rich dravite shown in Figure 2 in plane-polarized light (PPL) and X-ray fluorescence maps showing the distribution of Ni, Cr, Fe, Na, and Mg. Individual sectors |*hkl*| are labeled in the PPL image. A dark-colored concentric zone roughly at the center of the trigonal prism sectors is obvious in the PPL image.

Crystal-structure studies

Samples of Ni-bearing dravite were examined to determine the response of the atomic arrangement in tourmaline to the incorporation of Ni. Upon collection of three-dimensional X-ray data, refinement of the unit-cell parameters using 7,239 reflections measured on a well-aligned CCD detector yielded a γ angle *ca.* 119.8°; typical refinements of the unit-cell parameters on the instrument provided cell angles within 0.005° of the symmetry-constrained value. Furthermore, merging of the data showed that approximately 200 reflections violate the conditions of *R*-lattice centering. The results invited further examination, and several crystals that were subsequently examined also yielded similar deviations of the γ angle from the 120° of *R*3*m* tourmaline. The suggested break in symmetry from hexagonal *R*3*m* tourmaline motivated our optical studies, summarized above, perhaps the most simple and effective way of confirming reduction of hexagonal symmetry. Those studies yielded the definitive biaxial interference-figures that confirm the reduction of symmetry from hexagonal (Fig. 2).

Structure studies were undertaken on a Bruker Apex CCD diffractometer equipped with graphite-monochromated Mo*K*α radiation. Refined cell-parameters and other crystal data are listed in Table 1. Redundant data were collected for an approximate sphere of reciprocal space, and were integrated and corrected for Lorentz and polarization factors using the Bruker program SAINTPLUS (Bruker AXS Inc. 2003). The structure reported here appertains to a crystal fragment cut from the rim of one of the nickel-bearing tourmaline crystals. Although the exact sectoral volume that comprises the fragment is undetermined, given its size and the location from which it was taken, it is likely to be composed entirely or dominantly of a trigonal prism sector |100| or |010|.

The biaxial interference-figures of the Ni-bearing tourmaline result from symmetry reduction from the *R*3*m* space group of tourmaline. Biaxial subsymmetries of space group *R*3*m* are *Cm* (monoclinic) and *P*1 (triclinic); we selected space group *P*1 for the refinements, a choice that was affirmed for reasons given subsequently.

In the *R*3*m* space group of tourmaline, the following cation sites and ranks occur: *X*, rank 1; *Y*, rank 3; *Z*, rank 6; *T*, rank 6; and the *B* site, rank 3. In the triclinic subsymmetry-equivalent of tourmaline, each symmetry-equivalent site in tourmaline becomes an independent site, thus there is one *X* site, three unique *Y* sites, six unique *Z* and *T* sites, and three unique *B* sites. Evaluation of the dissymmetrization thus involves analysis of the differences in scattering values of the central cations and differences in the bond lengths of each of the subsymmetric polyhedra. To facilitate this comparison, the primitive triclinic cell used in this study [*a* 7.2304(4), *b* 9.4771(6), *c* 9.5188(6) Å, α 113.784(1), β 104.621(1), γ 104.576(1)°] was recast in the non-conventional space-group *R*1, defining a triply-primitive cell similar to the triply-primitive hexagonal *R* cell but not constrained to the hexagonal constraints of $a = b$, $\alpha = \beta = 90°$, $\gamma = 120°$.

The structure was solved using direct methods and difference-Fourier maps, as implemented in the Bruker SHELXTL V. 6.14 (Bruker AXS, Inc. 2000) package of programs; neutral-atom scattering factors and terms for anomalous dispersion were employed throughout the solution and refinement. Refinement was performed with anisotropic thermal parameters for all non-hydrogen atoms, and the structure was refined on F^2; the hydrogen atoms in the Ni-bearing tourmaline were successfully located with difference-Fourier maps. The unit-cell parameters are reported in Table 1, and the atom nomenclature (Table 2) corresponds to the traditional hexagonal cell. Table 2 also contains the site-occupancy factors and anisotropic displacement factors, and Table 3 contains a list of selected bond-lengths in the atomic arrangement. Tables of structure factors are available from the Depository of Unpublished Data on th MAC website [document Triclinic dravite CM49_29].

Wright *et al.* (2000) offered a method for using structure and chemical data to optimize the site occupancies of complex minerals. Applying methods of quadratic programming to the data for the nickel-bearing tourmaline, the occupancies of the three hexagonal-equivalent ^{Y}Al sites and the six hexagonal-equivalent ^{Z}Al sites were optimized; those occupancies are contained in Table 4. Also contained in Table 4 are the site scattering and mean bond-length for each of the nine octahedral sites, facilitating comparison among them. In the optimization, the ^{Z}Al-equivalent sites were constrained to have full occupancy, and the ^{Y}Al-equivalent sites were allowed to have vacancies, as have been noted in trigonal tourmalines.

Chemical studies

The crystal of dravite chosen for our structural investigation, measuring 50 × 50 × 65 μm, was analyzed

TABLE 1. CRYSTAL DATA AND RESULTS OF STRUCTURE REFINEMENT FOR Ni-BEARING DRAVITE

Unit-cell parameters by least squares (space group: *R*1, 7,239 reflections)
a 15.903(1) *b* 15.9118(8) *c* 7.2304(4) Å
α 90.063(2)° β 89.793(2)° γ 119.742(3) *V* 1588.57(18) Å^3
Frame width, scan time, number of frames: 0.20°, 15 s, 4500
Detector distance: 5 cm
Effective transmission: 0.808679 - 1.000
R_{int} (before, after SADABS absorption correction): 0.0494, 0.0317
Unique reflections, refined parameters: 6,039, 472
$R1 = 0.0441$ for 5817 $Fo > 4\sigma(Fo)$ and 0.0464 for all 6039 data
Largest difference peaks: +0.84, – 0.71 e$^-$ Å^{-3}
Goodness-of-fit: 1.133

TABLE 2. POSITIONS, SITE-OCCUPANCY FACTORS, AND ANISOTROPIC DISPLACEMENT PARAMETERS FOR ATOMS IN Ni-BEARING DRAVITE FROM THE MIDDLE URALS, RUSSIA

	x	*y*	*z*	sof	U_{11}	U_{22}	U_{33}	U_{23}	U_{13}	U_{12}	U_{eq}
Na1	0	0	1/4	0.96(1)	0.026(1)	0.028(1)	0.026(1)	0.004(1)	0.005(1)	0.013(1)	0.0267(1)
Sia	0.8575(2)	0.5240(2)	0.3510(4)	1.00000	0.0037(1)	0.0046(5)	0.0053(6)	0.0011(4)	0.0009(4)	0.0016(4)	0.0047(2)
Sib	0.6633(2)	0.5231(2)	0.3490(4)	1.00000	0.0051(5)	0.0047(5)	0.0057(6)	0.0004(4)	0.0010(4)	0.0030(4)	0.0050(2)
Sic	0.4768(2)	0.3355(2)	0.3508(4)	1.00000	0.0043(5)	0.0049(5)	0.0064(6)	0.0012(4)	0.0015(4)	0.0024(4)	0.0052(2)
Sid	0.8564(2)	0.3355(2)	0.3542(4)	1.00000	0.0046(5)	0.0052(5)	0.0056(5)	0.0017(4)	0.0002(4)	0.0029(4)	0.0049(2)
Sie	0.6634(2)	0.1423(2)	0.3543(4)	1.00000	0.0039(5)	0.0051(5)	0.0057(5)	0.0020(4)	0.0008(4)	0.0024(4)	0.0048(2)
Sif	0.4762(2)	0.1422(2)	0.3527(4)	1.00000	0.0044(5)	0.0048(5)	0.0060(6)	0.0020(4)	0.0016(4)	0.0028(5)	0.0049(2)
^{Y}Ala	0.6049(2)	0.3939(2)	-0.0125(4)	1.338(8)	0.0060(5)	0.0070(5)	0.0105(6)	-0.0003(4)	0.0021(4)	0.0020(4)	0.0084(3)
^{Y}Alb	0.7891(2)	0.3944(2)	-0.0098(4)	1.262(8)	0.0072(5)	0.0060(5)	0.0110(6)	0.0015(4)	-0.0009(4)	0.0038(4)	0.0078(4)
^{Y}Alc	0.6043(2)	0.2097(2)	-0.0088(4)	1.169(8)	0.0050(6)	0.0072(6)	0.0096(6)	0.0041(4)	0.0029(4)	0.0036(5)	0.0071(4)
^{Z}Ala	0.6305(2)	0.7026(2)	0.2960(4)	0.990(7)	0.0031(6)	0.0033(6)	0.0036(6)	-0.0000(4)	0.0005(4)	0.0014(5)	0.0034(4)
^{Z}Alb	0.9632(2)	0.7024(2)	0.6287(4)	1.025(7)	0.0037(6)	0.0051(6)	0.0053(7)	0.0019(4)	0.0021(4)	0.0020(5)	0.0048(4)
^{Z}Alc	1.0715(2)	0.7027(2)	0.2956(4)	1.008(7)	0.0052(6)	0.0050(6)	0.0040(7)	0.0006(4)	0.0006(4)	0.0029(5)	0.0046(4)
^{Z}Ald	0.7381(2)	0.7022(2)	0.6284(4)	1.011(7)	0.0066(7)	0.0072(7)	0.0073(7)	0.0021(5)	0.0011(5)	0.0047(5)	0.0065(4)
^{Z}Ale	0.9629(2)	0.2613(2)	0.6289(4)	0.998(7)	0.0027(6)	0.0059(7)	0.0047(7)	0.0024(4)	0.0018(4)	0.0024(5)	0.0043(4)
^{Z}Alf	0.9643(2)	0.5948(2)	-0.0380(4)	1.022(7)	0.0060(6)	0.0080(7)	0.0057(7)	0.0018(5)	0.0003(5)	0.0044(5)	0.0061(4)
B1	0.7805(4)	0.8905(4)	0.4686(8)	1.00000	0.009(2)	0.010(2)	0.008(2)	0.003(2)	0.002(2)	0.006(2)	0.0082(9)
B2	0.7752(4)	0.5522(4)	-0.1934(8)	1.00000	0.006(2)	0.009(2)	0.007(2)	0.002(2)	0.002(2)	0.004(2)	0.0075(8)
B3	0.1099(4)	0.8892(4)	0.4754(8)	1.00000	0.006(2)	0.006(2)	0.010(2)	0.005(2)	0.003(2)	0.001(2)	0.0081(9)
O1a	0.6653(3)	0.3307(3)	0.1192(5)	1.00000	0.013(1)	0.014(2)	0.013(2)	-0.001(1)	0.001(1)	0.008(1)	0.0127(6)
O2a	0.5448(3)	0.2700(3)	-0.1586(6)	1.00000	0.006(1)	0.011(1)	0.010(2)	0.003(1)	0.002(1)	0.003(1)	0.0010(6)
O2b	0.7259(3)	0.2699(3)	-0.1543(6)	1.00000	0.010(1)	0.012(1)	0.011(1)	0.003(1)	0.001(1)	0.008(1)	0.0100(6)
O2c	0.7278(3)	0.4539(3)	-0.1604(6)	1.00000	0.009(1)	0.007(1)	0.012(1)	-0.000(1)	0.002(1)	0.003(1)	0.0099(6)
O3a	0.5351(3)	0.4637(3)	-0.1352(6)	1.00000	0.014(2)	0.012(2)	0.003(2)	0.001(1)	0.001(1)	0.000(1)	0.0125(7)
H3a	0.529(4)	0.453(4)	-0.229(8)	1.00000	0.00(1)						
O3b	0.8763(3)	0.7469(4)	0.5287(7)	1.00000	0.017(2)	0.026(2)	0.005(2)	-0.000(1)	0.001(1)	0.013(2)	0.0148(7)
H3b	0.874(5)	0.744(5)	0.45(1)	1.00000	0.02(2)						
O3c	0.9251(3)	0.4605(3)	-0.1374(6)	1.00000	0.029(2)	0.020(2)	0.003(1)	0.001(1)	0.000(1)	0.020(2)	0.0138(7)
H3c	0.926(6)	0.460(6)	-0.251(1)	1.00000	0.05(4)						
O4a	0.7604(3)	0.5238(3)	0.4208(6)	1.00000	0.005(1)	0.016(2)	0.011(1)	0.000(1)	0.001(1)	0.007(1)	0.0100(6)
O4b	0.4790(3)	0.2406(3)	0.4255(6)	1.00000	0.021(2)	0.007(1)	0.011(2)	0.004(1)	0.004(1)	0.011(1)	0.0114(6)
O4c	0.7567(3)	0.2427(3)	0.4238(6)	1.00000	0.006(1)	0.008(1)	0.010(2)	0.003(1)	0.002(1)	-0.003(1)	0.0111(6)
O5a	0.5747(3)	0.4248(3)	0.4424(6)	1.00000	0.005(1)	0.006(1)	0.012(2)	0.003(1)	-0.003(1)	-0.001(1)	0.0091(6)
O5b	0.5714(3)	0.1463(3)	0.4485(5)	1.00000	0.008(1)	0.015(2)	0.009(1)	0.003(1)	0.001(1)	0.009(1)	0.0093(6)
O5c	0.8500(3)	0.4268(3)	0.4448(6)	1.00000	0.013(1)	0.007(1)	0.011(2)	0.002(1)	0.002(1)	0.007(1)	0.0093(6)
O6a	0.8593(3)	0.5164(3)	0.1291(6)	1.00000	0.014(2)	0.015(2)	0.007(1)	-0.001(1)	0.000(1)	0.009(1)	0.0110(6)
O6b	0.6548(3)	0.5166(3)	0.1270(6)	1.00000	0.011(1)	0.011(1)	0.006(1)	-0.002(1)	-0.002(1)	0.004(1)	0.0098(6)
O6c	0.6554(3)	0.1393(3)	0.1324(6)	1.00000	0.011(1)	0.012(2)	0.005(1)	0.003(1)	-0.001(1)	0.007(1)	0.0089(6)
O6d	0.8617(3)	0.3445(3)	0.1315(5)	1.00000	0.009(1)	0.009(1)	0.004(1)	0.003(1)	0.002(1)	0.005(1)	0.007(6)
O6e	0.4813(3)	0.3429(3)	0.1281(6)	1.00000	0.008(1)	0.009(1)	0.008(1)	0.003(1)	0.002(1)	0.004(1)	0.0085(6)
O6f	0.4853(3)	0.1433(3)	0.1326(6)	1.00000	0.011(1)	0.011(2)	0.008(1)	0.003(1)	0.005(1)	0.006(1)	0.0098(6)
O7a	0.6611(3)	0.6166(3)	0.4212(6)	1.00000	0.014(2)	0.008(1)	0.011(2)	0.001(1)	0.002(1)	0.007(1)	0.0102(6)
O7b	0.9524(3)	0.6191(3)	0.4257(5)	1.00000	0.006(1)	0.006(1)	0.007(1)	-0.002(1)	-0.002(1)	-0.001(1)	0.0081(6)
O7c	0.6685(3)	0.0509(3)	0.4318(6)	1.00000	0.010(1)	0.008(1)	0.011(2)	0.007(1)	0.004(1)	0.006(1)	0.0088(6)
O7d	0.3797(3)	0.0487(3)	0.4263(6)	1.00000	0.005(1)	0.007(1)	0.009(1)	0.002(1)	0.002(1)	0.003(1)	0.0072(6)
O7e	0.3823(3)	0.3351(3)	0.4271(6)	1.00000	0.004(1)	0.014(2)	0.014(2)	-0.001(1)	0.003(1)	0.005(1)	0.0107(6)
O7f	0.9468(3)	0.3308(3)	0.4354(6)	1.00000	0.011(1)	0.014(1)	0.010(2)	0.001(1)	-0.003(1)	0.009(1)	0.0103(6)
O8a	0.8742(3)	0.6019(3)	-0.2133(6)	1.00000	0.007(1)	0.012(2)	0.020(2)	0.006(1)	0.006(1)	0.006(1)	0.0123(7)
O8b	1.0620(3)	0.7907(3)	0.4573(6)	1.00000	0.007(1)	0.008(1)	0.012(2)	-0.003(1)	0.003(1)	0.001(1)	0.0100(6)
O8c	1.2088(3)	0.9398(3)	0.4606(6)	1.00000	0.007(1)	0.005(1)	0.010(2)	-0.001(1)	0.003(1)	0.001(1)	0.0084(6)
O8d	0.7297(3)	0.7924(3)	0.4452(6)	1.00000	0.011(1)	0.008(1)	0.015(2)	-0.002(1)	-0.004(1)	0.006(1)	0.0103(6)
O8e	1.0652(3)	0.6082(3)	0.1286(6)	1.00000	0.011(1)	0.007(1)	0.014(2)	-0.001(1)	-0.002(1)	0.006(1)	0.0100(6)
O8f	0.0591(3)	0.2678(3)	0.4669(6)	1.00000	0.009(2)	0.009(2)	0.015(2)	0.0038(1)	0.0032(1)	0.0054(1)	0.0107(6)

TABLE 3. SELECTED BOND-LENGTHS (Å) IN Ni-BEARING DRAVITE

Na1-	O2c	2.492(4)	Sia-	O6a	1.610(3)	Sib-	O7a	1.592(3)	Sic-	O7e	1.596(3)
	O2a	2.508(4)		O7b	1.612(3)		O6b	1.610(3)		O6e	1.613(3)
	O2b	2.543(4)		O4a	1.620(3)		O4a	1.626(3)		O4b	1.622(3)
	O5c	2.719(4)		O5c	1.639(3)		O5a	1.642(3)		O5a	1.641(3)
	O5a	2.725(4)	Mean		1.620(6)	Mean		1.618(6)	Mean		1.618(6)
	O4c	2.737(4)									
	O5b	2.763(4)	Sid-	O7f	1.590(3)	Sie-	O7c	1.599(3)	Sif-	O6f	1.597(3)
	O4b	2.835(4)		O6d	1.615(3)		O6c	1.609(3)		O7d	1.607(3)
	O4a	2.880(4)		O4c	1.620(3)		O4c	1.630(3)		O4b	1.630(3)
Mean		2.689(10)		O5c	1.641(3)		O5b	1.642(3)		O5b	1.639(3)
			Mean		1.617(6)	Mean		1.620(6)	Mean		1.618(6)
^{Y}Ala-	O1a	1.951(4)	^{Y}Alb-	O1a	1.945(4)	^{Y}Alc-	O1a	1.912(4)			
	O6b	1.981(3)		O6a	1.969(3)		O6f	1.936(3)			
	O6e	1.990(3)		O6d	1.981(3)		O6c	1.967(3)			
	O2c	2.003(3)		O2c	1.991(3)		O2a	1.974(3)			
	O2a	2.012(3)		O2b	2.013(3)		O2b	1.979(3)			
	O3a	2.119(4)		O3c	2.089(4)		O3b	2.020(4)			
Mean		2.009(8)	Mean		1.998(8)	Mean		1.965(8)			
^{Z}Ala-	O8d	1.862(3)	^{Z}Alb-	O8a	1.901(4)	^{Z}Alc-	O8b	1.886(3)			
	O7a	1.897(3)		O7b	1.926(3)		O8e	1.892(3)			
	O6d	1.906(3)		O6c	1.932(3)		O7c	1.894(3)			
	O7d	1.909(3)		O8b	1.944(3)		O6e	1.900(3)			
	O8c	1.918(3)		O7e	1.948(3)		O7b	1.933(3)			
	O3c	1.975(3)		O3b	1.978(4)		O3a	1.986(4)			
Mean		1.911(7)		Mean	1.938(8)	Mean		1.915(8)			
^{Z}Ald-	O8f	1.964(3)	^{Z}Ale-	O7f	1.880(3)	^{Z}Alf-	O6a	1.930(4)			
	O6f	1.984(3)		O8f	1.885(3)		O7e	1.933(3)			
	O7a	1.988(3)		O6b	1.904(3)		O8e	1.935(3)			
	O8d	2.007(3)		O8c	1.907(3)		O8a	1.962(4)			
	O7f	2.030(3)		O7d	1.954(3)		O7c	1.997(3)			
	O3b	2.073(4)		O3a	1.998(4)		O3c	2.037(4)			
Mean		2.008(8)	Mean		1.921(8)	Mean		1.966(9)			
B1-	O8d	1.367(6)	B2-	O8f	1.355(5)	B3-	O8b	1.367(6)			
	O8e	1.373(5)		O8a	1.374(6)		O8c	1.370(6)			
	O2a	1.380(6)		O2c	1.379(6)		O2b	1.373(6)			
Mean		1.373(10)	Mean		1.369(10)	Mean		1.370(10)			

with a Cameca SX–50 electron-microprobe (EMP) located at the Ruhr-Universität Bochum, Germany. The following operating conditions were used: 15 kV accelerating voltage, beam current 15 nA, and beam diameter of approximately 5 μm. Natural and synthetic silicate and oxide standards were used for calibration, and the data were reduced and corrected using the PAP routine (Pouchou & Pichoir 1985). The results of the optical absorption study demonstrate that nearly all Fe exists as Fe^{2+} in the sample from the crystal core, but a coexistence with hematite and the optimization of the atomic arrangement suggest that the iron in a significant portion of the edge of the crystal exists as Fe^{3+}. In Table 5, we report the chemical composition and the optimization using the Fe as Fe^{3+}, as suggested from the structure analysis, but note that the core of the crystal is dominantly Fe^{2+}, reinforcing the observation of Baksheev & Kudryavtseva (2004) that there is considerable heterogeneity in Fe oxidation state in the crystal.

X-ray-fluorescence maps (Fig. 3) of the distribution of Ni, Cr, Fe, Na, Mg, Si and Al were made on a (001) section using EDS on a Zeiss Supra35 scanning electron microscope at Miami University with an operating voltage of 20 kV. Maps were made at a 1024 × 800 spot resolution with a 200 microsecond dwell-time per spot, and 465 scans were summed.

TABLE 4. SITE OCCUPANTS, OBSERVED SITE-SCATTERING, AND MEAN BOND-LENGTH FOR OCTAHEDRAL SITES

Site	Occupants	Observed site-scattering (e^-)	Mean bond length (Å)
^{Y}Ala	$Al_{0.292}Mg_{0.344}Fe^{3+}_{0.364}$	17.4(1)	2.009(8)
^{Y}Alb	$Al_{0.375}Mg_{0.334}Cr^{3+}_{0.022}Fe^{3+}_{0.269}$	16.4(1)	1.998(8)
^{Y}Alc	$Al_{0.399}Mg_{0.098}Cr^{3+}_{0.238}Ni_{0.112}\square_{0.153}$	15.2(1)	1.965(8)
^{Z}Ala	$Al_{0.936}Mg_{0.064}$	12.87(9)	1.911(7)
^{Z}Alb	$Al_{0.801}Mg_{0.166}Ni_{0.033}$	13.33(9)	1.938(8)
^{Z}Alc	$Al_{0.946}Mg_{0.045}Ni_{0.010}$	13.10(9)	1.915(8)
^{Z}Ald	$Al_{0.387}Mg_{0.542}V^{3+}_{0.031}Fe^{3+}_{0.002}Ti^{4+}_{0.039}$	13.14(9)	2.008(8)
^{Z}Ale	$Al_{0.915}Mg_{0.082}Ni_{0.003}$	12.97(9)	1.921(8)
^{Z}Alf	$Al_{0.629}Mg_{0.316}Cr^{3+}_{0.055}$	13.29(9)	1.966(9)

The observed scattering was modeled using Al scattering curves.

RESULTS

Optical studies

Figures 1 and 3 show that six trigonal prism sectors, |100| and |010|, and a pedion sector comprise the (001) section. Figure 2 shows the (001) section in crossed polars at two different orientations, roughly 30° apart, and optical interference-figures taken within the |001| sector. The slightly off-center acute bisectrix interference-figure, *Bxa*, indicates that the section is roughly four degrees from a true (001) orientation. The optic angle varies throughout the section from approximately 4 to >10°, and all areas exhibit a negative optic sign. The optical orientation also varies throughout the section. Domains of different optical orientation, indicated by different extinction-angles and $2V$, correspond directly to trigonal prism {100}, {010} and pedion {001} sectors, indicating optical sectoral zoning. Irregular domains of different optical orientation and undulatory extinction are observed within some sectors. Color differences exist between the pedion and trigonal prism sectors, as seen in the plane-polarized light (PPL) image in Figure 3. A dark-colored concentric zone that lies roughly at the center of the trigonal prism sectors is also obvious in the PPL image.

Elemental zoning

Figure 3 shows the X-ray fluorescence maps of the distribution of Ni, Cr, Fe, Na, and Mg. Both Si and Al show a homogeneous distribution throughout the section, and maps for them are not shown here. Given the orientation of the (001) section, concentric compositional boundaries (resulting from concentric zoning) within the |001| sector will be approximately parallel to the section. Concentric zones within the trigonal-prism sectors, however, will be oriented 90° to the section; thus multiple concentric zones will be exposed in these sectors. The concentric zone in the prism sectors that is coeval with the one exposed in the pedion sector is directly adjacent to the pedion sector (*i.e.*, the innermost concentric zone in the prism sectors). The distribution of Ni, Cr and Fe in the prism sectors show clear indication of concentric zoning. Although they may exist, these data do not clearly show differences in concentration between coeval portions of the symmetrically nonequivalent sectors (*i.e.*, compositional sectoral zoning). The distribution of Na and Mg is different from that of Ni, Cr and Fe. There is no obvious concentric zoning within the prism sectors, nor is there an observable difference in concentration between nonequivalent prism-sectors. There is, however, a distinct difference in concentration between the prism sectors and the pedion sector.

Origin of the color

The presence of Ni in this tourmaline invites speculation as to whether the green color derives from its nickel content. The optical absorption spectrum of the Ni-bearing dravite (Fig. 4) has strong absorptions in the 400, 600–700, and 1100 nm regions, in addition to OH features near 1450, 2300, and 2700 nm. The strong pleochroism reported by Baksheev & Kudryavtseva (2004) is consistent with the much greater intensity of absorption in the **E** ⊥ **c** direction seen in the spectrum. The absorption spectrum of Ni^{2+} in olivine (Rossman *et al.* 1981) has a band near 410 nm, near 780 nm, and

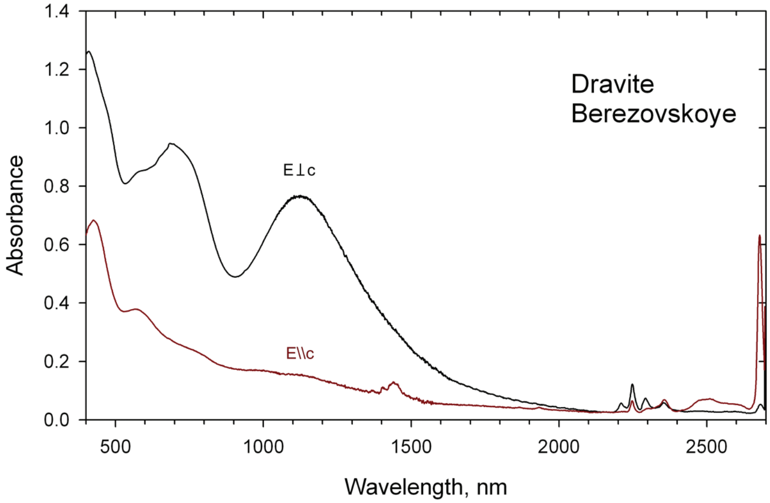

FIG. 4. Optical absorption spectrum of the Berezovskoye tourmaline obtained through a 79 × 415 μm area of the darkest-colored portion of a 78.5 μm thick crystal. Absorption from Fe and Cr dominate the spectrum.

in the 1200–1500 nm region. Thus Ni is a candidate for the origin of color. However, because Ni, Cr, and Fe are all present in the Berezovskoe tourmaline, each of these elements must be considered as the source of color.

The role of Ni

Nickel in sixfold coordination in oxides generally produces green colors. The solid-state spectra of Ni in a variety of crystals have been studied by Rossman *et al.* (1981); in the simplest case of cubic NiO, the Ni^{2+} spectrum consists of three bands in the regions of 430 nm, 680 nm, and 1140 nm.

The strong pleochroism in this sample of dravite may not be due to nickel. According to Taran (1993), "pleochroism is practically absent" in their synthetic Ni-bearing tourmaline. The likelihood that the 1125 nm band in the Berezovskoe tourmaline sample comes from Ni can be tested by comparing the intensity of its 1125 nm band to the intensity of the 1060 nm band in the Taran (1993) sample. Ignoring minor differences in density, this comparison indicates that there is 42 times too much intensity in the Berezovskoe tourmaline's absorption at 1125 nm to be due to Ni. A similar comparison to the 775 nm band indicates that there is 45 times too much absorption.

TABLE 5. CHEMICAL COMPOSITION AND EMPIRICAL FORMULA OF Ni-BEARING DRAVITE

SiO_2 wt.%	35.43(23)	Si *apfu*	5.85
TiO_2	0.19(8)	$^{[4]}Al$	0.15
B_2O_3[1]	10.52	Sum *T* site	6
Al_2O_3	29.83(94)		
Cr_2O_3	2.31(76)	$^{[3]}B$	3
V_2O_3	0.13(6)		
Fe_2O_3[2]	5.01(89)	Al	5.66
MnO	0.01(1)	Cr^{3+}	0.3
MgO	8.14(21)	V^{3+}	0.02
ZnO	0.02(1)	Fe^{3+}	0.62
NiO	1.10(45)	Mg	2
CoO	0.02(1)	Ti^{4+}	0.02
CaO	0.09(1)	Ni	0.15
Na_2O	2.82(5)	Sum *Y*, *Z* sites	8.77
K_2O	0.03(1)		
H_2O[3]	3.63	Ca	0.02
		Na	0.9
Sum	99.28	K	0.01
		□	0.07
		Sum *X* site	1
		Sum cations	18.70
		OH	4
		F	0
		Sum OH + F	4

Note: Average result of eight EMP analyses. [1] B_2O_3 calculated as B = 3.00 *apfu*. [2] Fe calculated as Fe^{3+} (see text). [3] H_2O calculated as OH = 4.00 *pfu*. F is below the detection limit.

The role of Cr

In the spectrum of Cr-bearing dravite, the Cr absorption is near 600 nm and 430 nm with **E** ⊥ **c** somewhat more intense than **E** ǁ **c** (Ertl *et al.* 2008). Comparison of the 620 nm intensity to GRR2467 (Ertl *et al.*) and Tourmaline 10 in Taran *et al.* (1993) shows that the intensity of the 620 nm bands in the Berezovskoe crystal have only 61 and 67% of the expected intensity, respectively, based on the reported Cr_2O_3 contents of the samples. We can attribute this to inhomogeneity in the Berezovskoe sample. This, however, does show that no contributions from Ni are required to account for the intensity in the 620 nm (and 400 nm) regions.

The role of Fe

The role of iron also must be considered. In Fe-containing tourmalines, Fe^{2+} bands are found in the 1100 and 700 nm regions. In tourmalines with mixed Fe oxidation states, the intensities can be much greater in the **E** ⊥ **c** direction (Mattson & Rossman 1987). For example, the intensities of the 1105 nm band in the spectrum of the green portion of tourmaline S5 of Mattson & Rossman (1987) can be used to estimate the possible intensity of bands due to Fe for the Berezovskoe tourmaline. The intensity of tourmaline S5 is 173 cm^{-1} in the **E** ⊥ **c** polarization. After normalizing for different FeO concentrations, the equivalent band in the Berezovskoe tourmaline could be as much as 112 cm^{-1}, a factor of 1.4 times greater than the observed band. The actual intensity will depend on the ratio of Fe^{2+} to Fe^{3+}. This result immediately indicates that Fe^{2+} absorptions alone could account for all the absorption in the 1100 (and 700 nm regions). More specifically, a contribution from Ni^{2+} is not required.

Baksheev & Kudryavtseva (2004) demonstrated that there is significant heterogeneity in the Fe oxidation state in the dravite. We selected a sample from the core to evaluate the Fe^{2+}:Fe^{3+} ratio in that, the darkest portion of the crystal; an estimate of the amount of Fe^{3+} in contact with Fe^{2+} in the Berezovskoe tourmaline can be obtained. Firstly, the molar absorptivity of the 1125 nm Fe band must be determined. Using the absorbance of 77.9 per cm thickness, an estimated density of 3.10 g/cm^3, and the Fe_2O_3 concentration of 5.01 wt%, a molar absorptivity of 40.0 is calculated. From Figure 6 of Mattson & Rossman (1987), which relates the molar absorptivity of the 1100 nm band to the fraction of adjacent Fe^{2+}–Fe^{3+} pairs, we estimate that only 3% of the iron in the core of the Berezovskoe crystal need be in the form of adjacent Fe^{2+}–Fe^{3+} pairs.

In summary, we conclude that the color in the **E** ⊥ **c** polarization comes dominantly from Fe mixed-oxidation state couples, and from Cr^{3+}. Contributions from the nickel are believed to be minor and will fall in the regions of strong Cr and Fe absorption.

CRYSTAL-STRUCTURE STUDIES

In the single previous investigation of the structure of triclinic tourmaline, Shtukenberg *et al.* (2007) found that the dissymmetrization resulted from non-equivalency at the tourmaline *Y* sites due to cation ordering. In contrast to that study, the current study on Ni-bearing tourmaline demonstrates that dissymmetrization results from non-equivalency at both the *Y* and *Z* sites. Table 4 lists the site occupants, site-scattering values, and mean bond-lengths for each of the octahedral sites, and illustrates the nature of the break in symmetry.

In contrast to the three hexagonally equivalent tourmaline *Y* sites, marked differences occur at the triclinic sites (^{Y}Ala–^{Y}Alc). As noted in Table 4, the difference in site occupancies among the three sites yield significantly different values in mean bond-length and site scattering, illustrating how the *Y* sites can, through dissymmetrization, provide environments for a variety of substituents. The difference in site-scattering and mean bond-lengths, and concomitantly in site occupants, confirm the choice of triclinic symmetry, as in monoclinic symmetry two of the *Y* sites would be related by a mirror plane. We can compare the differences in site-scattering values and mean bond-lengths for the three sites (in terms of sigmas of the observation): ^{Y}Ala–^{Y}Alb: 10σ in site scattering, 1.4σ in mean bond-length, ^{Y}Alb–^{Y}Alc: 12σ in site scattering, 4.1σ in mean bond-length, and ^{Y}Ala–^{Y}Alc: 22σ in site scattering, 5.5σ in mean bond-length. The differences in site-scattering values and mean bond-lengths confirm the choice of space group *P*1, cast in the non-conventional form *R*1.

In the structure study of triclinic tourmaline by Shtukenberg *et al.* (2007), the authors noted that the symmetry break occurred solely from differences among the *Y* sites. However, in our Ni-bearing tourmaline, there are significant differences in occupancy among the hexagonal-equivalent *Z* sites, as well. Table 4 illustrates the remarkable range in mean bond-length and cation occupancy among the *Z* sites. In particular, the ^{Z}Ald site occupants illustrate how the cation sites, through dissymmetrization, are robust and can accommodate a variety of cation substituents. The six *Z* sites are equivalent in the *R*3*m* tourmaline atomic arrangement, but in the *R*1 structure, they are symmetrically distinct. The ^{Z}Ala and ^{Z}Ald sites, symmetrically equivalent in *R*3*m* but symmetrically distinct in *R*1, illustrate the results of the symmetry break in this Ni-bearing tourmaline. As noted in Table 4, the ^{Z}Ala site hosts $Al_{0.935}Mg_{0.065}$ and has a mean bond-length of 1.911(7) Å, whereas the ^{Z}Ald site hosts $Al_{0.386}Mg_{0.542}V^{3+}_{0.032}Ti^{4+}_{0.039}$ and has a mean bond-length of 2.008(8) Å; clearly the dissymmetrization of tourmaline has a large effect on the atomic arrangement of tourmaline.

DISCUSSION

The causes of optical anomalies in tourmaline and other minerals include internal stress arising from defects and compositional heterogeneities (Foord & Mills 1978, Gorskaya *et al.* 1992, Shtukenberg & Punin 2007). A second cause of anomalous optical behavior is dissymmetrization due to ordering. In many minerals, such dissymmetrization may occur as a post-growth order-related phase transition (Dove 1999, Putnis 1992). However, in others, including tourmaline, dissymmetrization can occur during crystal growth as a result of differential incorporation of cations and anions among structurally different atomic sites on the surface that in the bulk crystal are structurally identical (Bulka *et al.* 1980, Akizuki *et al.* 2001, Shtukenberg *et al.* 2007, Shtukenberg & Punin 2007).

Akizuki *et al.* (2001) found that in optically sectorally zoned liddicoatite–elbaite, the |101|, |021|, |100| sectors are optically biaxial and triclinic, |110| sectors are optically biaxial and orthorhombic, and the |001| sector is uniaxial and trigonal. The biaxial, triclinic nature of the |100| sectors is similar to that found in this study; however, comparable properties are observed in the |001| sector in contrast to that found by Akizuki *et al.* (2001). The coincidence of domains with different optical properties with growth sectors was interpreted to indicate that dissymmetrization occurs during crystal growth. Small, optically anomalous domains and wavy extinction in some sectors may be the possible result of local strain within the crystals.

In the single previous structural study of triclinic tourmaline (Shtukenberg *et al.* 2007), space group *R*1 was determined on the basis of an analysis of X-ray-diffraction data and structure refinement, which showed that the dissymmetrization was the result of Al and Li ordering among the *Y* octahedral sites. They observed that the degree of Al–Li order correlates with 2*V*, and suggested a causal relationship. Based on the sectoral distribution of domains of different optical character and an analysis of observed *Y*-site ordering compared to crystal-face symmetry and growth mechanism, Shtukenberg *et al.* (2007) proposed that Al–Li order results from geometrical differences of the *Y* octahedral sites as they are exposed at the crystal surface. These differences lead to differential incorporation among the different surface-sites. The resulting ordered arrangement lowers the symmetry of the bulk structure, leading to the anomalous optical behavior.

The observed optical anomalies in this study are similar to those reported by Akizuki *et al.* (2001) and Shtukenberg *et al.* (2007), indicating dissymmetrization due to differential incorporation during growth among structurally different atomic sites on the surface that in the bulk crystal are structurally identical. Localized heterogeneities in optical behavior, such as undulatory extinction in some domains, are attributed to strain. All bulk crystallographic sites in a mineral structure can have different surface manifestations depending on geometry, orientation, the specific crystal faces present, and the orientation of growth steps and other microtopographic features on the surface. In contrast to the results of Shtukenberg *et al.* (2007), the observed order in this study indicates that structural heterogeneities among both the surface *Y* and *Z* sites leads to differential incorporation and dissymmetrization.

Future researchers should be aware of the possibility of lower symmetry in tourmaline, and the concomitant ability of the atomic arrangement to incorporate a wide variety of cation substituents by adjusting its apparently robust atomic arrangement. Such detailed observations may indicate a newly recognized role for tourmaline in trace- and minor-element variation in rocks in which the phase crystallizes.

ACKNOWLEDGMENTS

This work was supported in part by National Science Foundation (U.S.A) grants EAR–0003201 to JMH and EAR–0337816 to GRR. Darrell Henry and an anonymous reviewer provided insightful and valuable comments on the work, and Editor-in-Chief Robert F. Martin provided his typical outstanding review; sincere thanks to all. This work was supported in part by Österreichischer Fonds zur Förderung der wissenschaftlichen Forschung (FWF) project no. P20509–N10.

REFERENCES

AKIZUKI, M., KURIBAYASHI, T., NAGASE, T. & KITAKAZE, A. (2001): Triclinic liddicoatite and elbaite in growth sectors of tourmaline from Madagascar. *Am. Mineral.* **86**, 364-369.

BAKSHEEV, I.A. & KUDRYAVTSEVA, O.E. (2004): Nickeloan tourmaline from the Berezovskoe gold deposit, Middle Urals, Russia. *Can. Mineral.* **42**, 1065-1078.

BRUKER AXS, INC. (2000): SHELXTL v. 6.14 Software Package. Madison, Wisconsin, U.S.A.

BRUKER AXS, INC. (2003): SaintPlus v. 6.45 Software Package. Madison, Wisconsin, U.S.A.

BULKA, G.R., VINOKUROV, V.M., NIZAMUTDINOW, N.M. & HASANOVA, N.M. (1980): Dissymmetrization of crystals: theory and experiment. *Phys. Chem. Minerals* **6**, 283-293.

DIETRICH, R.V. (1985): The *Tourmaline Group*. New York, Van Nostrand Reinhold Co., New York, N.Y.

DOVE, M.T. (1999): Order/disorder phenomena in minerals: ordering phase transitions and solid solutions. *In* Microscopic Properties and Processes in Minerals (C.R.A. Catlow & K. Wright, eds.). Kluwer Academic Publishers, Dordrecht, The Netherlands (451-475).

ERTL, A., ROSSMAN, G.R., HUGHES, J.M., MA, CHI & BRANDSTÄTTER, F. (2008): V^{3+}-bearing, Mg-rich, strongly disordered olenite from a graphite deposit near Amstall, Lower Austria: a structural, chemical and spectroscopic investigation. *Neues Jarhb. Mineral., Abh.* **184**, 243-253.

FOORD, E.E. & MILLS, B.A. (1978): Biaxiality in "isometric" and "diametric" crystals. *Am. Mineral.* **63**, 316-325.

GORSKAYA, M.G., PUNIN, Y.O., SOKOLOV, P.B. & KREZER, Y.A. (1992): Compositional inhomogeneity and heterometry in the crystals of polychromic tourmalines. *Mineral. Zh.* **14**(3), 8-20 (in Russian).

HENRY, D.J. & DUTROW, B.L. (2001): Compositional zoning and element partitioning in nickeloan tourmaline from a metamorphosed karstbauxite from Samos, Greece. *Am. Mineral.* **86**, 1130-1142.

HENRY, D.J., KIRKLAND, B.L. & KIRKLAND, D.W. (1999): Sector-zoned tourmaline from the cap rock of a salt dome. *Eur. J. Mineral.* **11**, 263-280.

MATTSON, S.M. & ROSSMAN, G.R. (1987) Fe^{2+}–Fe^{3+} interactions in tourmaline. *Phys. Chem. Minerals* **14**, 163-171.

POUCHOU, J.L. & PICHOIR F. (1985): 'PAP' $\phi(\rho Z)$ procedure for improved quantitative microanalysis. *In* Microbeam Analysis (J.T. Anderson, ed.). San Francisco Press, San Francisco, California (104-106).

PUTNIS, A. (1992): *Introduction to Mineral Sciences*. Cambridge University Press, New York, N.Y.

ROSSMAN, G.R., SHANNON, R.D. & WARING, R.K. (1981): Origin of the yellow color of complex nickel oxides. *J. Solid State Chem.* **39**, 277-287.

RUSTEMEYER, P. (2003) *Faszination Turmalin*. Spektrum Akademischer Verlag, Heidelberg, Germany.

SHTUKENBERG, A. & PUNIN, Y.O. (2007): *Optically Anomalous Crystals*. Springer, Dordrecht, The Netherlands.

SHTUKENBERG, A., ROZHDESTVENSKAYA, I., FRANK-KAMENETSKAYA, O., BRONZOVA, J., EULER, H., KIRFEL, A., BANNOVA, I. & ZOLOTAREV, A. (2007): Symmetry and crystal structure of biaxial elbaite–liddicoatite tourmaline from the Transbaikalia region, Russia. *Am. Mineral.* **92**, 675-686.

TARAN, M.N., LEBEDEV, A.S. & PLATONOV, A.N. (1993): Optical absorption spectroscopy of synthetic tourmalines. *Phys. Chem. Minerals* **20**, 209-220.

VAN HINSBERG, V.J. & MARSCHALL, H.R. (2007): Boron isotope and light element sector zoning in tourmaline; implications for the formation of B-isotopic signatures. *Chem. Geol.* **238**, 141-148.

VAN HINSBERG, V.J., SCHUMACHER, J.C., KEARNS, S., MASON, P.R.D. & FRANZ, G. (2006): Hourglass sector zoning in metamorphic tourmaline and resultant major and trace element fractionation. *Am. Mineral.* **91**, 717-728.

WRIGHT, S.E., FOLEY, J.A. & HUGHES, J.M. (2000): Optimization of site occupancies in minerals using quadratic programming. *Am. Mineral.* **85**, 524-531.

Received November 19, 2009, revised manuscript accepted January 9, 2011.